Journal of Solid State Chemistry 182 (2009) 1045–1054

Contents lists available at ScienceDirect

Journal of Solid State Chemistry

journal homepage: www.elsevier.com/locate/jssc

Solvothermal synthesis and luminescent properties of monodisperse $LaPO_4$:*Ln* (*Ln* = Eu^{3+}, Ce^{3+}, Tb^{3+}) particles

Piaoping Yang [a,b], Zewei Quan [a], Chunxia Li [a], Zhiyao Hou [b], Wenxin Wang [b], Jun Lin [a,*]

[a] State Key laboratory of Rare Earth Resource Utilization, Changchun Institute of Applied Chemistry, Chinese Academy of Sciences, Changchun 130022, PR China
[b] College of Material Science and Chemical Engineering, Harbin Engineering University, Harbin 150001, PR China

ARTICLE INFO

Article history:
Received 15 October 2008
Received in revised form
16 January 2009
Accepted 22 January 2009
Available online 30 January 2009

Keywords:
Solvothermal synthesis
Luminescence
$LaPO_4$
Monodisperse

ABSTRACT

Monodisperse rare-earth ion (Eu^{3+}, Ce^{3+}, Tb^{3+}) doped $LaPO_4$ particles with oval morphology were successfully prepared through a facile solvothermal process without further heat treatment. X-ray diffraction (XRD), scanning electron microscopy (SEM), transmission electron microscopy (TEM), X-ray photoelectron spectra (XPS), Fourier transform infrared spectroscopy (FT-IR), photoluminescence (PL) spectra and the kinetic decays were performed to characterize these samples. The XRD results reveal that all the doped samples are well crystalline at 180 °C and assigned to the monoclinic monazite-type structure of the $LaPO_4$ phase. It has been shown that all the as-synthesized samples show perfectly oval morphology with narrow size distribution. The possible growth mechanism of the $LaPO_4$:*Ln* has been investigated as well. Upon excitation by ultraviolet radiation, the $LaPO_4$:Eu^{3+} phosphors show the characteristic $^5D_0$–$^7F_{1-4}$ emission lines of Eu^{3+}, while the $LaPO_4$:Ce^{3+}, Tb^{3+} phosphors demonstrate the characteristic $^5D_4$–$^7F_{3-6}$ emission lines of Tb^{3+}.

1. Introduction

Nowadays, the synthesis of inorganic materials with nanometer dimensions and hierarchical morphologies has gained much attention in modern nanoscale science and technology, which shows potential applications in the fields of catalysis, separation technology, microelectronic devices, and biomaterials engineering [1–7]. The structural characteristics such as the size, morphology and the surface compositions of the products have a significant effect on the physicochemical properties, which can be tuned in a controllable manner to tailor their magnetic, optical, mechanical, thermal, electrical, electro-optical, and catalytic properties [8–15]. In particular, the phosphor particles with sphere-like morphology, suitable particle size range (0.5–2 μm), non-agglomeration, and monodisperse size distribution are of special interest in the new display fields such as plasma display panel (PDP) and field emission display (FED) due to their brighter high definition, cathodoluminescent performance, and much improved screen packing [16,17]. So far, a variety of synthetic approaches have been developed to control the morphology and size of the phosphor particles, such as spray pyrolysis [18], sol–gel process [19], and urea homogeneous precipitation [20]. However, the obtained phosphor particles fabricated via these routines are still far away from the ideal morphology, so it is still a challenge to seek a facile synthetic method to achieve this goal.

Lanthanide compounds have been extensively used as optoelectronic devices, magnets, catalysts, and biological fluorescence labeling because of their special optical, electronic, and chemical properties resulting from the 4f electron configurations [21–25].

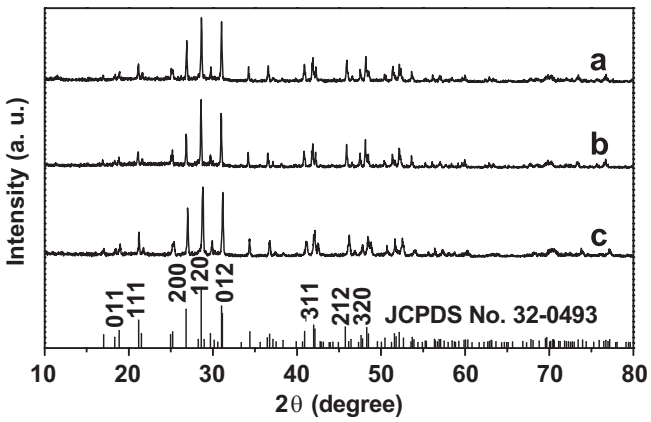

Fig. 1. XRD patterns of the as-synthesized $LaPO_4$:Eu^{3+} (a), $LaPO_4$:Ce^{3+}, Tb^{3+} (b), $LaPO_4$:Ce^{3+}, Tb^{3+} (c) phosphors, and the standard data for bulk $LaPO_4$ (JCPDS 32–0493).

* Corresponding author at: State Key laboratory of Rare Earth Resource Utilization, Changchun Institute of Applied Chemistry, Chinese Academy of Sciences, Changchun 130022, PR China. Fax: +86 431 85698401.
E-mail address: jlin@ciac.jl.cn (J. Lin).

0022-4596/$ - see front matter © 2009 Elsevier Inc. All rights reserved.
doi:10.1016/j.jssc.2009.01.024

In recent years, lanthanide orthophosphates ($LnPO_4$) have attracted much interest for the potential applications as phosphors, proton conductors, sensors, catalysts, ceramic materials, and heat-resistant materials [26] based on their interesting properties, such as low water solubility [27], high thermal stability [28], high index of refraction, and high concentrations

Table 1
Unit cell lattice constants for $LaPO_4:Eu^{3+}$, $LaPO_4:Ce^{3+}$, and $LaPO_4:Ce^{3+}$, Tb^{3+}.

Samples	*a*/deviation (nm)	*b*/deviation (nm)	*c*/deviation (nm)	β angle/deviation (deg)	Cell volume/deviation (nm^3)
JCPDS 32–0493	0.6837	0.7077	0.6509	103.23	0.3065
$LaPO_4:Eu^{3+}$	0.6831/0.0006	0.7061/0.0016	0.6502/0.0007	103.66/0.43	0.3059/0.0006
$LaPO_4:Ce^{3+}$	0.6829/0.0008	0.7062/0.0015	0.6501/0.0008	103.73/0.50	0.3051/0.0014
$LaPO_4:Ce^{3+}$, Tb^{3+}	0.6828/0.0009	0.7058/0.0019	0.6498/0.0011	103.62/0.39	0.3047/0.0018

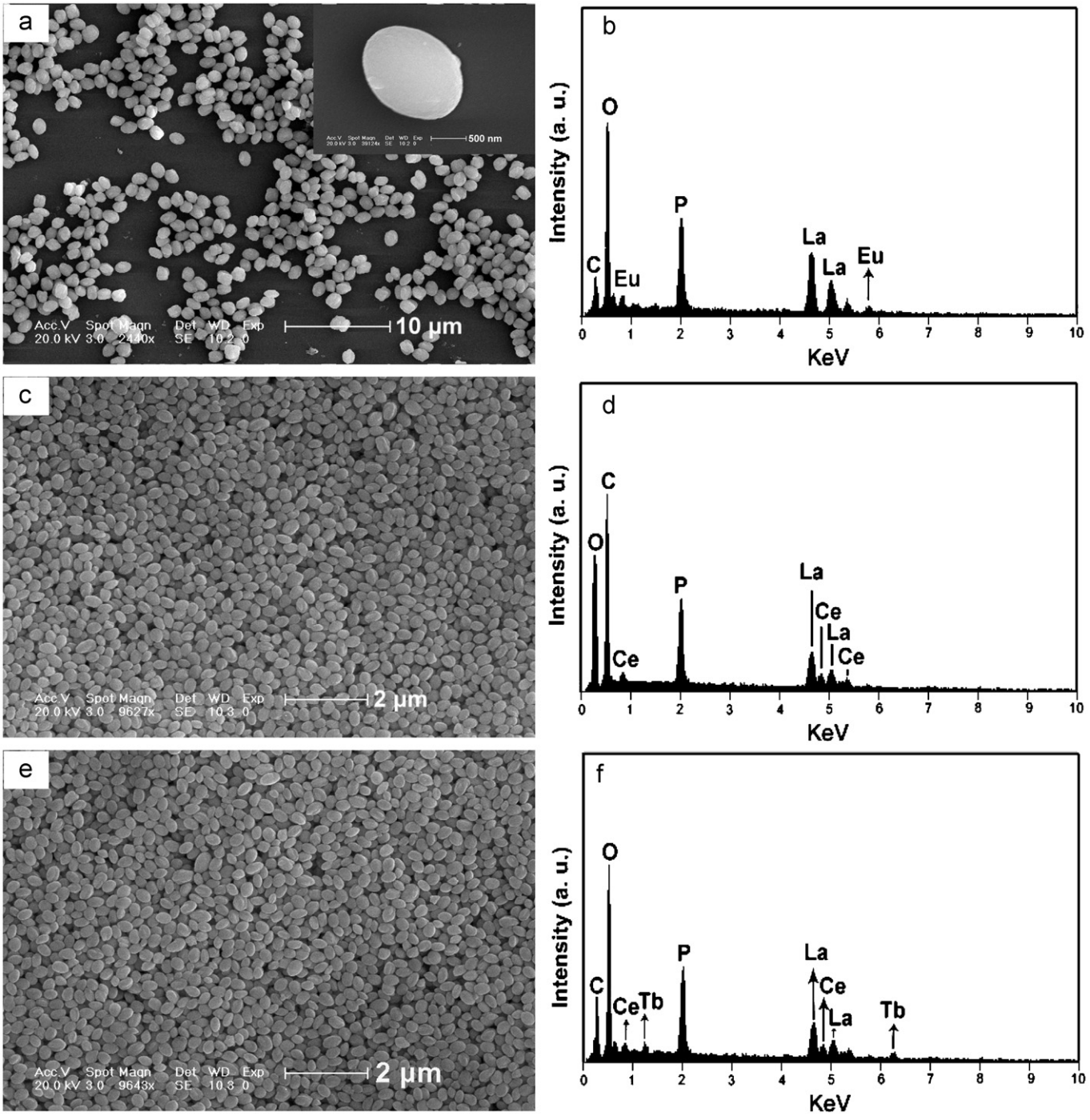

Fig. 2. SEM images of the as-synthesized $LaPO_4:Eu^{3+}$ (a), $LaPO_4:Ce^{3+}$ (c), $LaPO_4:Ce^{3+}$, Tb^{3+} (e) phosphors and the corresponding EDS (b, d, f).

of lasing ions [29], and so on. Furthermore, lanthanide phosphates have been shown to be a useful host lattice for doping lanthanide ions to prepare phosphors emitting a wide range of colors [30–32]. As a highly efficient green ($^5D_4$–$^7F_5$ of Tb^{3+} at 544 nm) phosphor, Ce^{3+} and Tb^{3+} co-activated bulk $LaPO_4$ powders have been extensively applied to fluorescent lamps and PDPs due to the high energy transfer efficiency between Ce^{3+} and Tb^{3+} [33–35]. The luminescent properties of this phosphor strongly depend on the compositions and structure, which are sensitive to the bonding states of lanthanide ions. Over the past decade, $LaPO_4$:Eu^{3+}, $LaPO_4$:Ce^{3+}, $LaPO_4$:Ce^{3+}, Tb^{3+} as well as $CePO_4$:Tb^{3+}/$LaPO_4$ (core–shell) with various morphologies have been fabricated through a large variety of routines, including hydrothermal method [36–38], wet chemical precipitation [39], microwave approach [40], sol–gel process [41,42], ultrasonic irradiation [43], and polyol-mediated method [44]. The products obtained through such processes are usually nanowires or nanofibers with one dimension (1D). However, the shape controlled synthesis of rare-earth ions doped $LaPO_4$ with uniform sphere-like morphology via a solvothermal process has rarely been reported. The solvothermal process can produce a highly crystalline and homogenous product without post-calcination obtained at a mild reaction conditions (reaction temperature $<250\,^{\circ}C$). At the same time, the morphologies of the products can be controlled by altering the synthesis conditions.

In this paper, a facile solvothermal process was proposed for the synthesis of monodisperse rare-earth ion (Eu^{3+}, Ce^{3+}, Tb^{3+}) doped $LaPO_4$ phosphor particles with uniformly oval morphology and narrow size distribution. The obtained samples were well characterized by means of X-ray diffraction (XRD), Field emission scanning electron microscopy (FESEM), transmission electron microscopy (TEM), X-ray photoelectron spectra (XPS), infrared spectroscopy (IR), optical spectra as well as the kinetic decay times. A possible growth mechanism for the micro-sized particles has also been proposed.

2. Experimental section

2.1. Synthesis of $LaPO_4$:Eu^{3+}, $LaPO_4$:Ce^{3+} and $LaPO_4$:Ce^{3+}, Tb^3

All the reagents for synthesis including ethylene glycol (EG; A. R., Beijing Fine Chemical Company), $(NH_4)_2HPO_4$ (Beijing Chemical Regent Company), NaOH (A. R., Beijing Chemical Regent Company), La_2O_3, Eu_2O_3, Tb_4O_7, $Ce(NO_3)_3 \cdot 6H_2O$ (99.99%, Science and Technology Parent Company of Changchun Institute of Applied Chemistry), HNO_3 (A. R., Beijing Beihua Chemical Company) were purchased without further purification. The doping concentration of Eu^{3+} was 5 mol% to La^{3+} in $LaPO_4$:Eu^{3+}, which has been optimized [45]. In a typical process, 0.95 mmol La_2O_3 and 0.05 mmol Eu_2O_3 were dissolved in dilute HNO_3 with vigorous stirring. The superfluous HNO_3 was driven off until the pH value of the solution reached between 2 and 3. Then the $Eu(NO_3)_3$ and $La(NO_3)_3$ crystal powders were obtained. Then the obtained $Eu(NO_3)_3$ and $La(NO_3)_3$ powders were added into the mixed solution of EG and water with the volume ratio of 37 to 3 with stirring. After further stirring for another 2 h, the resulting solution was then transferred into a 50 mL sealed Teflon autoclave and statically heated at 180 °C for certain time. After the autoclave was naturally cooled to the room temperature, the final products were separated by centrifugation, and washed several times with ethanol and distilled water. Finally, the obtained samples were dried in vacuum at 60 °C for 24 h. In this way, the Eu^{3+} doped $LaPO_4$ was obtained, which was designated as $LaPO_4$:Eu^{3+}. The $LaPO_4$:Ce^{3+} with the doping concentration of 20 mol% of Ce^{3+} to La^{3+} and the $LaPO_4$:Ce^{3+}, Tb^{3+} with the doping concentration of 20 mol% of Ce^{3+} and 15 mol% of Tb^{3+} to La^{3+} were prepared in the same process except for the doped rare-earth ion of Eu^{3+} has been replaced by Tb^{3+} and/or Ce^{3+}.

2.2. Characterization

Powder XRD patterns were obtained on a Rigaku TR III diffractometer using Cu$K\alpha$ radiation ($\lambda = 0.15405$ nm). Fourier-transform IR spectra were recorded on a Perkin–Elmer 580B IR spectrophotometer using KBr pellet technique. FESEM study was performed on a XL30 microscope (Philips) equipped with an energy-dispersive X-ray spectrum (EDS, JEOL JXA-840). TEM and high-resolution TEM (HRTEM) images were recorded on a FEI Tecnai G2 S-Twin with an acceleration voltage of 200 kV. The X-ray photoelectron spectra (XPS) were taken on a VG ESCALAB MK II electron energy spectrometer using Mg$K\alpha$ (1253.6 eV) as the X-ray excitation source. The exact doping concentrations of Eu^{3+}, Ce^{3+} and Tb^{3+} in the resulting materials were determined by inductively coupled plasma (ICP) performed on an ICP-PLASMA 1000 apparatus. The UV–vis excitation and emission spectra were obtained on a Hitachi F-4500 spectrofluorimeter equipped with a 150 W xenon lamp as the excitation source. Luminescence decay curves were obtained from a Lecroy Wave Runner 6100 Digital Oscilloscope (1 GHz) using a 250 nm laser (pulse width = 4 ns,

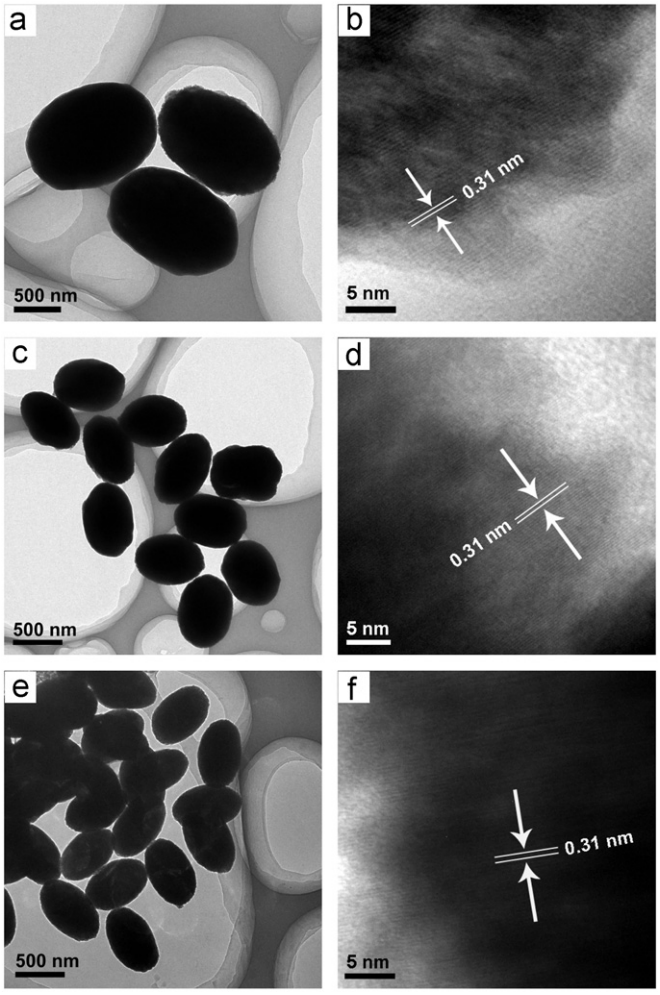

Fig. 3. TEM images of the as-synthesized $LaPO_4$:Eu^{3+} (a), $LaPO_4$:Ce^{3+} (c), $LaPO_4$:Ce^{3+}, Tb^{3+} (e) phosphors and the corresponding HRTEM images (b, d, f).

gate = 50 ns) as the excitation source (Continuum Sunlite OPO). All the measurements were performed at room temperature.

3. Results and discussion

3.1. Structure, formation, morphology and luminescent properties of $LaPO_4:Eu^{3+}$, $LaPO_4:Ce^{3+}$, $LaPO_4:Ce^{3+}$, Tb^{3+}

Fig. 1 show the XRD patterns of $LaPO_4:Eu^{3+}$, $LaPO_4:Ce^{3+}$, $LaPO_4:Ce^{3+}$, Tb^{3+} prepared at 180 °C for 12 h and the standard data for the monoclinic $LaPO_4$, respectively. It can be seen that the diffraction peaks of all the samples can be readily indexed to the monoclinic monazite-type structure of the $LaPO_4$ phase in $P2_1/n$ space group (JCPDS 32–0493). No additional peaks for other phases associated with the doped component can be detected, indicating that the as-synthesized samples are of pure monazite phase and rare-earth ions have been uniformly incorporated into the host lattice of $LaPO_4$. The calculated lattice constants of the synthesized samples are summarized in Table 1, together with a comparison with those of the JCPDS 32–0493 standard. It can be seen that the calculated cell lattice constants for $LaPO_4:Eu^{3+}$, $LaPO_4:Ce^{3+}$, and $LaPO_4:Ce^{3+}$, Tb^{3+} are well consistent with the standard data (JCPDS 32–0493). Furthermore, the actual doping concentration of Eu^{3+} in $LaPO_4:Eu^{3+}$ is 3.21 wt%; Ce^{3+} in $LaPO_4:Ce^{3+}$ is 11.92 wt% and Tb^{3+}, Ce^{3+} in $LaPO_4:Ce^{3+}$, Tb^{3+} is 9.98 and 11.73 wt% determined by ICP analysis, which are very close to the stoichiometric values (3.23 wt% or 5 mol% of Eu^{3+} in $LaPO_4:Eu^{3+}$, 11.97 wt% or 20 mol% of Ce^{3+} in $LaPO_4:Ce^{3+}$, 10.05 wt% or 15 mol% of Tb^{3+} and 11.82 wt% or 20 mol% of Ce^{3+} in $LaPO_4:Ce^{3+}$, Tb^{3+}).

The morphology and the microstructural details of the as-synthesized samples were further examined with SEM and TEM techniques. Fig. 2 displayed the SEM images of $LaPO_4:Eu^{3+}$, $LaPO_4:Ce^{3+}$, and $LaPO_4:Ce^{3+}$, Tb^{3+} prepared at 180 °C for 12 h as well as their corresponding EDS spectra, respectively. It can be seen from Fig. 2(a) that the $LaPO_4:Eu^{3+}$ phosphors consist of monodisperse oval particles with the mean size of about 1.5 μm in length and 1 μm in width. The EDS spectrum (Fig. 2(b)) of $LaPO_4:Eu^{3+}$ confirms the presence of lanthanum (La), phosphorous (P), oxygen (O), and europium (Eu) in the $LaPO_4:Eu^{3+}$ sample (the carbon signal is due to the carbon used as reference). The approximate composition of the products as extracted from the EDS analysis gives a Eu/La/P/O atomic ratio of 0.04:0.96:1:4.1, which is much consistent with the ICP results. From the SEM images of $LaPO_4:Ce^{3+}$ prepared at 180 °C for 12 h, we can see that the samples are composed of uniform oval particles with the particle size of about 500 nm in length and 300 nm in width. These particles are non-aggregated with smooth surface and narrow distribution. In the EDS spectrum (Fig. 2(d)), the signals of lanthanum (La), phosphorous (P), oxygen (O), and cerium (Ce) demonstrate the presence of the corresponding element in the

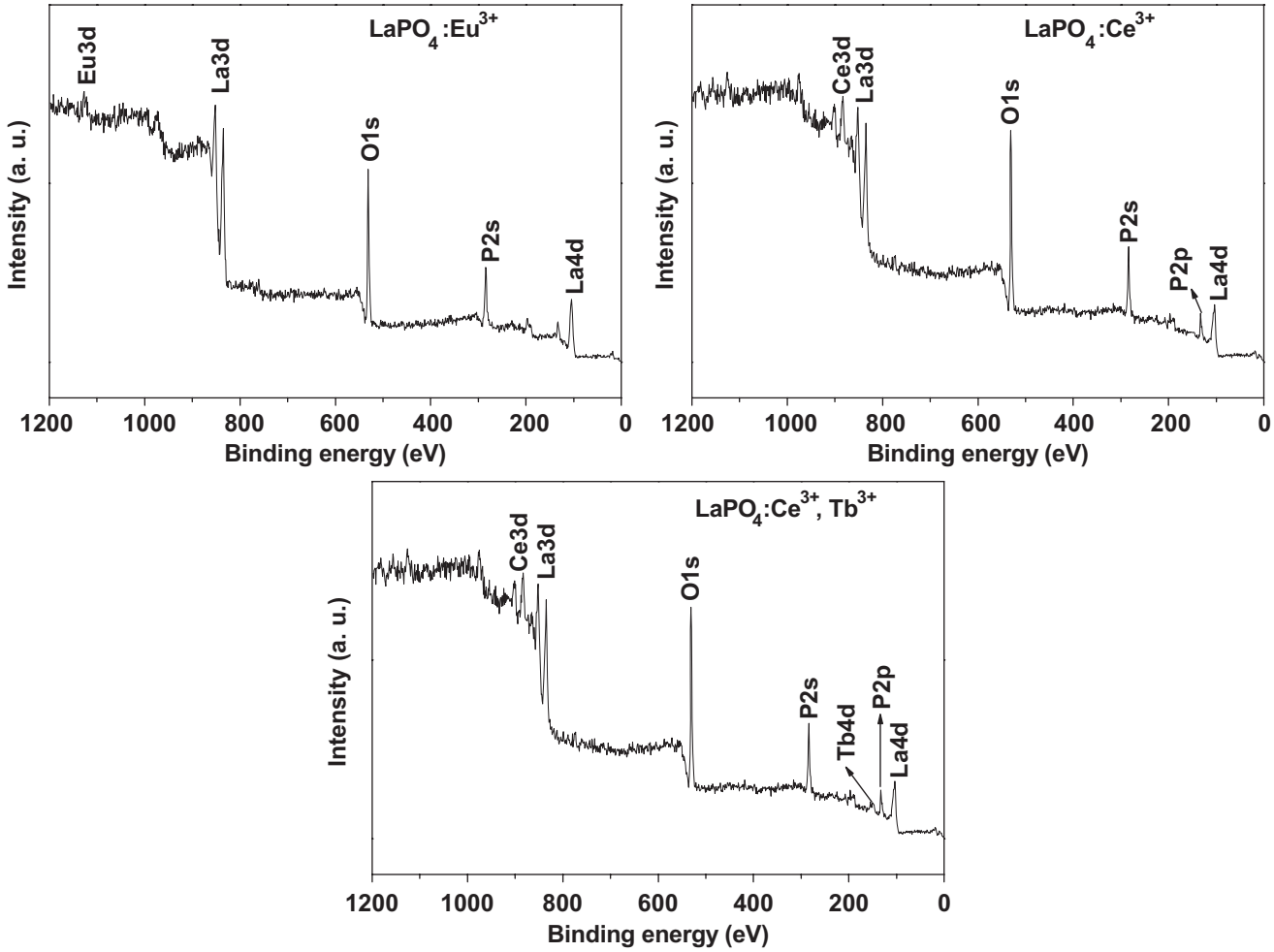

Fig. 4. XPS spectra for the as-synthesized $LaPO_4:Eu^{3+}$, $LaPO_4:Ce^{3+}$, and $LaPO_4:Ce^{3+}$, Tb^{3+} phosphors.

$LaPO_4:Ce^{3+}$ product. The approximate composition of the products extracted from the EDS analysis shows a Ce/La/P/O atomic ratio of 0.19:0.81:1:4.1, which is in good agreement with the ICP results. The morphology of the $LaPO_4:Ce^{3+}$, Tb^{3+} product (Fig. 2(e)) is much similar to that of $LaPO_4:Ce^{3+}$. Different from the EDS of $LaPO_4:Ce^{3+}$, the signal of Tb 4*d* is obvious in the EDS spectrum of $LaPO_4:Ce^{3+}$, Tb^{3+}. Additionally, the EDS analysis gives the approximate composition of 0.14/0.19/0.60/1/4.1 of Tb/Ce/La/O/P molar ratio, agreeing well with the ICP results.

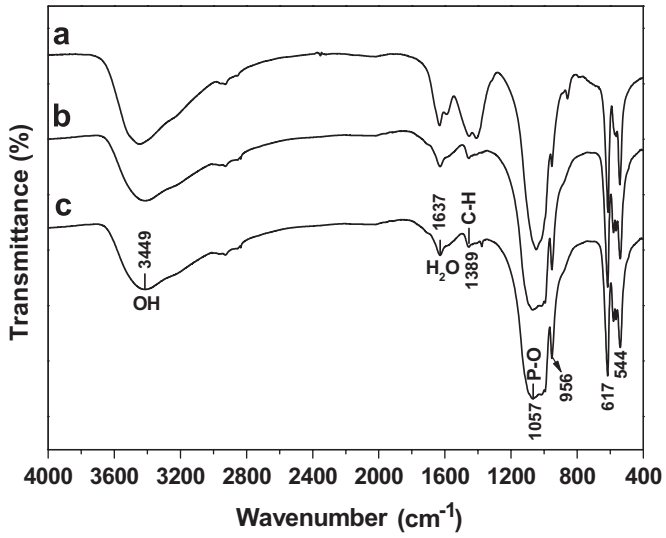

Fig. 5. FT-IR spectra of the as-synthesized $LaPO_4:Eu^{3+}$ (a), $LaPO_4:Ce^{3+}$ (b), and $LaPO_4:Ce^{3+}$, Tb^{3+} (c) phosphors.

Fig. 3 shows the representative TEM and HRTEM images of $LaPO_4:Eu^{3+}$, $LaPO_4:Ce^{3+}$, and $LaPO_4:Ce^{3+}$, Tb^{3+}, which highlight typically morphological and structural features. TEM images clearly indicate that monodisperse oval particles with uniform size distribution are obtained for all the samples, which are well consistent with the SEM results. The TEM results reveal that the doping components have little effect on the morphology of the samples, while the particle sizes of the phosphors are influenced greatly. The obvious lattice fringes in the HRTEM images (Fig. 3(b), (d) and (f)) confirm the high crystallinity of as-synthesized $LaPO_4:Eu^{3+}$, $LaPO_4:Ce^{3+}$ and $LaPO_4:Ce^{3+}$, Tb^{3+} phosphors, respectively. The lattice fringes of (120) planes with an interplanar distance of 0.31 nm are marked by the arrow in Fig. 3(b), (d) and (f). The calculated interplanar distance agrees well with the XRD analysis. The HRTEM images present a powerful tool to confirm the formation of well-crystallized single crystals.

XPS technique has been proven a powerful tool for qualitatively determining the surface component and composition of a material. The XPS spectra of $LaPO_4:Eu^{3+}$, $LaPO_4:Ce^{3+}$, and $LaPO_4:Ce^{3+}$, Tb^{3+} are shown in Fig. 4, respectively. The binding energy data (calibrated using C 1*s* (284.7 eV) as the reference) from the $LaPO_4:Eu^{3+}$, $LaPO_4:Ce^{3+}$, and $LaPO_4:Ce^{3+}$, Tb^{3+} are well consistent with those reported for bulk $LaPO_4$ [37,40]. The peaks at about 835, 885, and 1132 eV show the binding energies of the $3d_{5/2}$ orbital of La^{3+}, Ce^{3+}, and Eu^{3+} in the corresponding $LaPO_4:Ln$ products. The peak at about 133 eV (P 2*p*) for all the $LaPO_4:Ln$ phosphors indicates that the phosphorus in the products exists in a pentavalent oxidation state (P^{5+}) in the form of PO_4^{3-}.[37,46]. Additionally, the binding energy Tb (4*d*, 151.1 eV) is also obvious (Fig. 4c). By combination of the XRD results, it can be deduced that these signals can be assigned to the $LaPO_4:Ln$ phosphors.

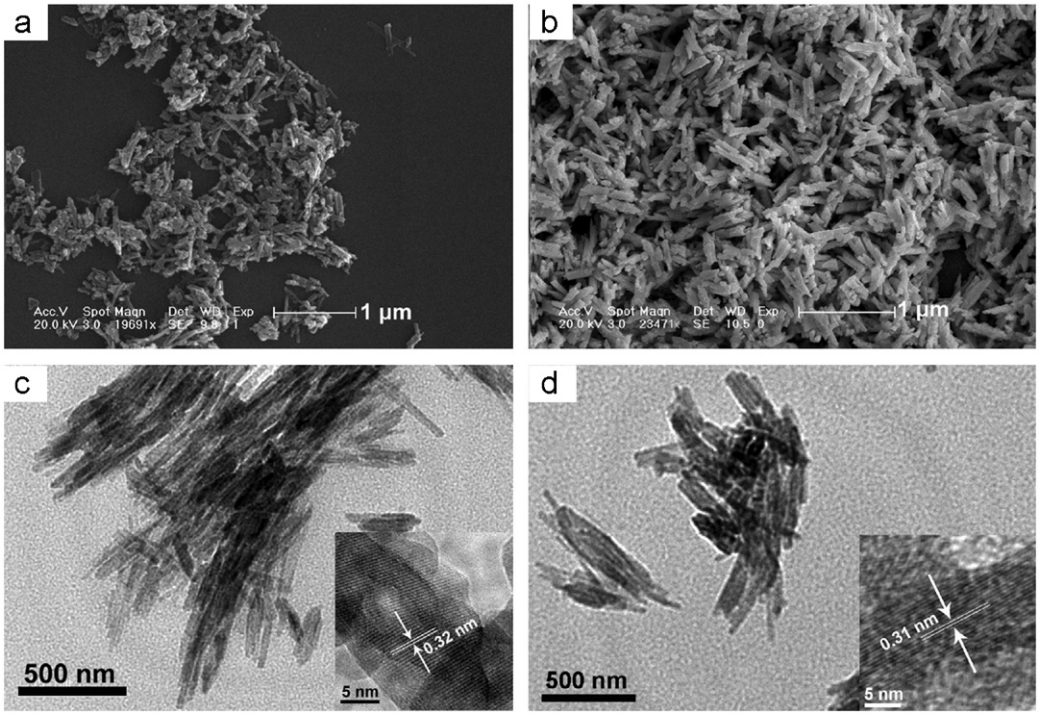

Fig. 6. SEM images of the as-synthesized $LaPO_4:Ce^{3+}$, Tb^{3+} phosphors synthesized with EG/H_2O volume ratio of $EG/H_2O = 0/40$ (a), $EG/H_2O = 30/10$ (b); TEM images of the as-synthesized $LaPO_4:Ce^{3+}$, Tb^{3+} phosphors synthesized with EG/H_2O volume ratio of $EG/H_2O = 0/40$ (c), $EG/H_2O = 30/10$ (d) and their corresponding HRTEM images (inset).

The FT-IR spectra for $LaPO_4:Eu^{3+}$, $LaPO_4:Ce^{3+}$, $LaPO_4:Ce^{3+}$, Tb^{3+} are depicted in Fig. 5, respectively. The absorption bands at 3449 and 1637 cm^{-1} can be assigned to physical adsorbed OH and H_2O for all the samples. The characteristic vibrations of phosphate (PO_4^{3-}) are obvious. The two bands located at 617 and 544 cm^{-1} are clearly observed in the v_4 region of the vibrations of PO_4^{3-} groups. The bands at 1057 cm^{-1} can be attributed to the v_3 anti-symmetric stretching of P–O band. The shoulder at 956 cm^{-1} can be assigned to the v_1 vibration of PO_4^{3-} groups [47]. The v_2 vibration at low wavenumber is not observed in the studied range of wave numbers. Furthermore, C–H stretching vibration at 1389 cm^{-1} can be detected, indicating the incomplete removal of the EG molecules from the surface of the samples.

3.2. The formation mechanism for the micrometer $LaPO_4$:Ln phosphors

The monodisperse and high-crystalline $LaPO_4$:*Ln* particles with uniform oval morphology may probably be formed through a mechanism which is similar to that for the preparation of $La(OH)_3$, CdSe, and Y_2O_3:Eu [48–50]. In this mechanism, if the overall growth rate is fast, the anisotropic growth rate is usually faster along a certain axis, resulting in the formation of long rod-like particle or the 1D nanosized materials. When the overall growth rate is slow, the isotropic growth is generally predominant, inducing the formation of sphere-like particles. Furthermore, EG has been widely used as an effectively protective agent to control the growth rate of the particles in the hydrothermal process. Thus, the size and morphology of the final products should be tuned by altering the concentrations of the EG and H_2O. Fig. 6 shows the typical SEM, TEM and their corresponding HRTEM images (inset) of $LaPO_4:Ce^{3+}$, Tb^{3+} prepared with different volume ratio of EG to H_2O. It is observed that rod-like particles with the particle size of about 500 nm in length and 50 nm in width are obtained when only pure H_2O (EG/H_2O volume ratios of $\frac{0}{40}$) was used in the same synthesis conditions (Fig. 6(a) and (c)). From the HRTEM image in Fig. 6(c, inset), the obvious lattice fringes and the good matching of the interplanar distance (0.31 nm) with the d_{120} value suggest the high crystallinity of the as-synthesized sample. When the EG/H_2O volume ratio is tuned to $\frac{30}{10}$, well-crystalline and relatively uniform rod-like particles with particle size of 0.5–1 μm in length are formed during the hydrothermal process, as shown in Fig. 6(b) and (d). When the volume ratio of EG/H_2O is increased to $\frac{37}{3}$, homogenous oval particles are achieved (Fig. 2(d)). Therefore, it can deduced that the volume ratio of EG/H_2O is a critical factor in influencing the size and morphology of the final product. This can be explained as following process. When only pure water or a small mount of EG was used as the synthesis medium, the growth rate of initial precursor along the *c*-axis is faster, resulting in the formation of rod-like particles without the protection of EG. When the concentration of EG is increased, the micro reactor where the nuclei and crystallinity occur is covered with EG by adsorption on the surface of the crystallites, which greatly hinder the growth rate of precursor particles along the *c*-axis. When the concentration of EG is high enough (EG/H_2O volume ratio of $\frac{37}{3}$), the EG molecules thoroughly adsorb on the crystal surfaces, which enhance the isotropic growth in all directions, so uniform oval micrometer-sized particles are obtained. To further investigate the growing process of the products, a series of tests have been employed. Fig. 7 gives the SEM images of $LaPO_4:Eu^{3+}$ synthesized at 180 °C for different reaction time. It can be seen that the particle size of the samples increase from 500 nm to 2 μm in length with the increment of the reaction time from 2 to 24 h, while the uniformly oval morphology is maintained. For the $LaPO_4:Ce^{3+}$, Tb^{3+} phosphors, the particle size also increases from 500 nm to 1 μm during the same reaction time range (Fig. 8), which is much similar to that of $LaPO_4:Eu^{3+}$. The SEM results indicate an obvious growing process from primary nanoparticles to the final larger products through self-assembly. A possible schematic illustration for the formation mechanism of $LaPO_4:Eu^{3+}$ is presented in Scheme 1.

3.3. Photoluminescence properties

As shown in Fig. 9, the $LaPO_4:Eu^{3+}$ and $LaPO_4:Ce^{3+}$, Tb^{3+} phosphors show brightly red and green luminescence under the

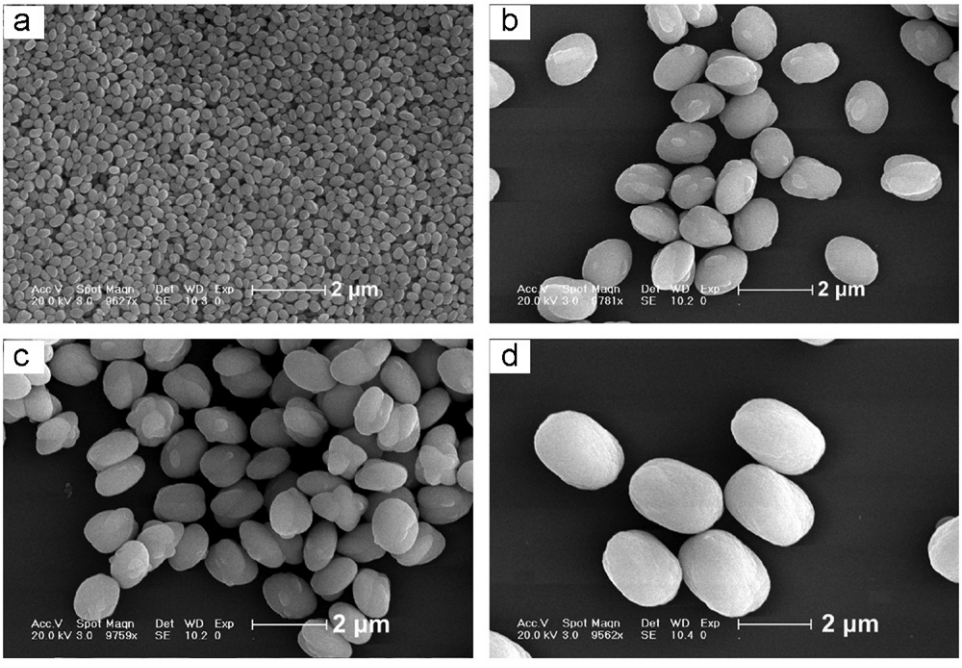

Fig. 7. SEM images of the as-synthesized $LaPO_4:Eu^{3+}$ phosphors synthesized at 180 °C for 2 h (a), 8 h (b), 12 h (c), and 24 h (d).

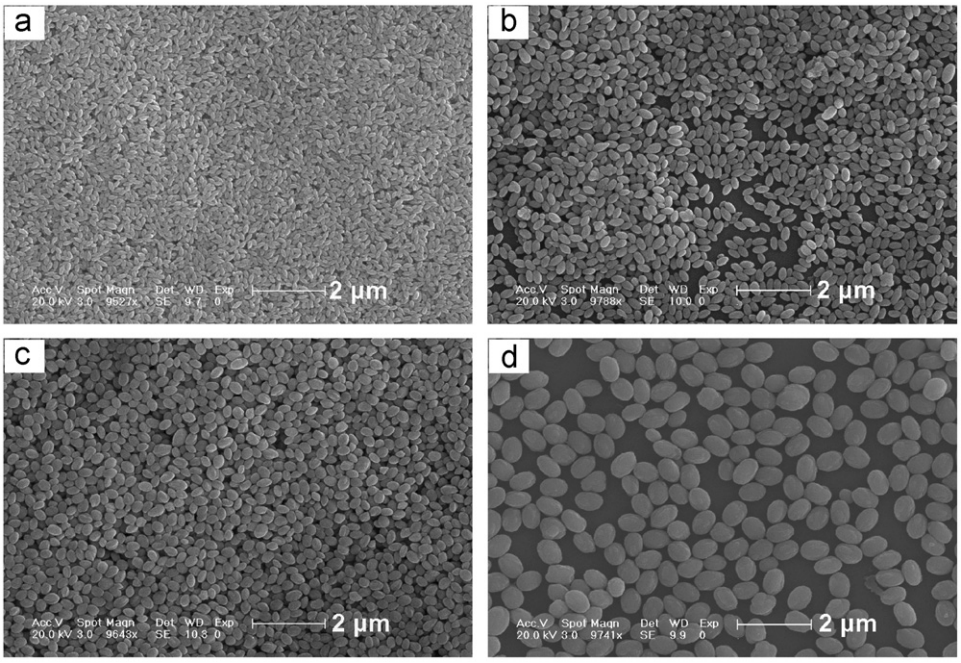

Fig. 8. SEM images of the as-synthesized $LaPO_4$:Ce^{3+}, Tb^{3+} phosphors synthesized at 180 °C for 2 h (a), 8 h (b), 12 h (c), and 24 h (d).

ultraviolet irradiation at 365 nm. Fig. 9 also exhibits the PL excitation and emission spectra of $LaPO_4$:Eu^{3+}, $LaPO_4$:Ce^{3+} and $LaPO_4$:Ce^{3+}, Tb^{3+}, respectively. In the excitation spectrum (Fig. 9(a)) monitored by the Eu^{3+} $^5D_0$–$^7F_2$ transition at 590 nm, the broad band with a maximum at 252 nm originates from the excitation of the oxygen-to-europium charge transfer band (CTB). The weak line at 396 nm may arise from *f*–*f* transitions within the Eu^{3+} $4f^6$ electron configuration [51], which corresponds to the direct excitation of the Eu^{3+} ground state into higher levels of the 4*f*-manifold ($^7F_0$–$^5L_6$) [37]. Upon excitation at 252 nm, the emission spectrum of the $LaPO_4$:Eu^{3+} product (Fig. 9(b)) is composed of the characteristic transition lines between Eu^{3+} levels. The locations and their assignments of the emission lines are labeled in the Fig. 9(b). Among $^5D_0$–^7F_J ($J = 1, 2, 3, 4$) emission lines of Eu^{3+}, the magnetic-dipole transition $^5D_0$–$^7F_1$ (590 nm) is the most prominent group. Furthermore, no emission from the higher energy levels ($^5D_1$, $^5D_2$) of Eu^{3+} can be detected because of the multiphoton relaxation derived from the vibration of phosphate groups, which can bridge the gaps between the lowest $^5D_0$ level of Eu^{3+} and the higher energy levels ($^5D_1$, $^5D_2$) effectively. The luminescent properties of Eu^{3+} in the crystalline $LaPO_4$ phosphors are in good agreement with those obtained through other processes [37,45], indicating that Eu^{3+} ions have been successfully doped into the host lattice of $LaPO_4$. Fig. 9(c) and (d) give the excitation and emission spectra for the luminescence of Ce^{3+} in $LaPO_4$:Ce^{3+} phosphors. In the excitation spectrum monitored by the emission wavelength of 341 nm, the spectrum (Fig. 9(c)) consists of a broad peak with maxima at 276 nm and two weak peaks at 217 and 241 nm, which correspond to the transitions from the ground state $^2F_{5/2}$ of Ce^{3+} to the different components of the excited Ce^{3+} 5*d* states split by the crystal field (in the $LaPO_4$ host lattice, the La^{3+} ion is surrounded by nine oxygen atoms with a site symmetry of C_1 [52]. The emission of Ce^{3+} in $LaPO_4$:Ce^{3+} shows a broad band with maxima at 341 nm, which are assigned to the parity-allowed transitions of the lowest component of the 2D state to the spin–orbit components of the ground state of Ce^{3+}. Fig. 9(e) and (f) shows the excitation and emission spectra for the luminescence of Tb^{3+} in the $LaPO_4$:Ce^{3+},

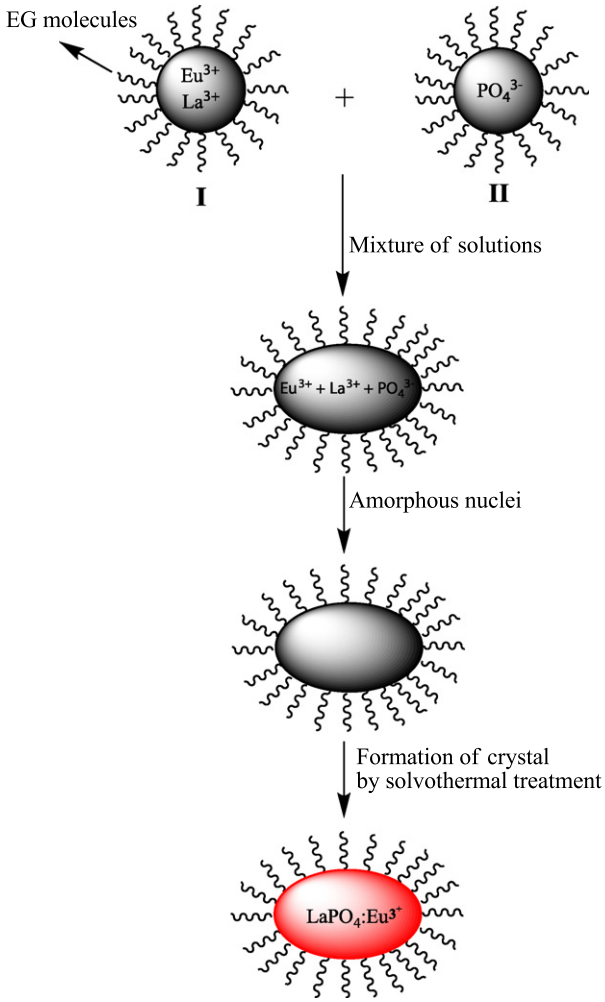

Scheme 1. Illustration for the formation process of $LaPO_4$:Eu^{3+} phosphors with oval morphology.

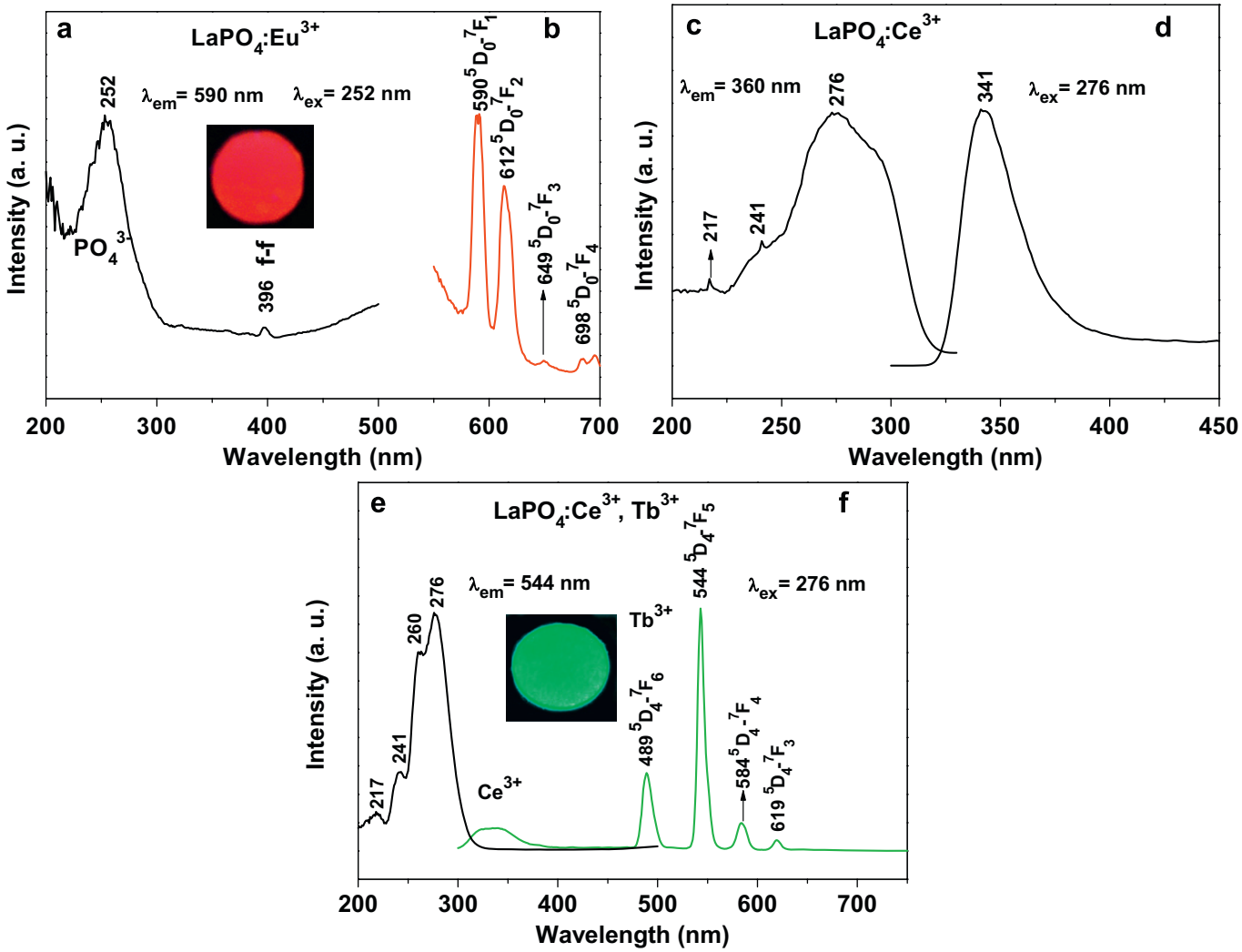

Fig. 9. The excitation (a, c, e) and emission (b, d, f) spectra of $LaPO_4:Eu^{3+}$ (a, b), $LaPO_4:Ce^{3+}$ (c, d), and $LaPO_4:Ce^{3+}$, Tb^{3+} (e, f).

Tb^{3+} phosphors. The excitation spectrum (Fig. 9e) monitored at the 544 nm ($^5D_4$–$^7F_5$) of Tb^{3+} consists of the excitation bands of Ce^{3+}, which is very similar to the excitation spectrum of Ce^{3+} in $LaPO_4:Ce^{3+}$ (Fig. 9(c)). Excitation into the Ce^{3+} band at 276 nm yields both the weak emission of Ce^{3+} (300–360 nm) and the strong emission of Tb^{3+} at 489 ($^5D_4$–$^7F_6$), 544 ($^5D_4$–$^7F_5$), 584 ($^5D_4$–$^7F_4$), and 619 nm ($^5D_4$–$^7F_3$), suggesting an efficient energy transfer from Ce^{3+} to Tb^{3+} in the $LaPO_4:Ce^{3+}$, Tb^{3+} phosphors. All the above spectral properties for the $LaPO_4:Ce^{3+}$, Tb^{3+} phosphors are basically consistent with the literatures [37,45,52].

Fig. 10 shows the decay curves for the $LaPO_4:Eu^{3+}$, $LaPO_4:Ce^{3+}$, $LaPO_4:Ce^{3+}$, Tb^{3+} phosphors, respectively. It can be seen that the decay curves for $^5D_0$–$^7F_2$ (612 nm) of Eu^{3+} can be well fitted into a single-exponential function as $I(t) = I_0 \exp(-t/\tau)$ (where τ is the $1/e$ lifetime of the Eu^{3+} ion) [53]. The lifetime of $^5D_0$ level of Eu^{3+} is 2.1 ms determined by this fitting. Like the single exponential luminescence decay of the $^5D_0$–$^7F_2$ transition of Eu^{3+} in the $LaPO_4:Eu^{3+}$ phosphors, the luminescence decay curves of Ce^{3+} in $LaPO_4:Eu^{3+}$ and Tb^{3+} in $LaPO_4:Ce^{3+}$, Tb^{3+} can also be fitted to a single exponential function, and the lifetimes of Ce^{3+} and Tb^{3+} is 11.4 ns and 1.55 ms, respectively. The luminescence lifetime of Tb^{3+} ($^5D_4$) in the range of milliseconds may be due to the forbidden nature of the *f*–*f* transition.

4. Conclusions

In summary, rare-earth ion (Eu^{3+}, Ce^{3+}, Tb^{3+}) doped $LaPO_4$ phosphor particles have been successfully obtained by a simple solvothermal process using EG as protective agent without further heat treatment. The obtained phosphor particles have homogenous oval morphology, non-agglomeration, monodisperse, and narrow size distribution. The obtained $LaPO_4:Eu^{3+}$ and $LaPO_4:Ce^{3+}$, Tb^{3+} phosphors show the characteristic emission lines of Eu^{3+} and Tb^{3+}, respectively. The decay curves of all the samples fit well into a single-exponential function. The possible formation mechanism for the $LaPO_4$:*Ln* has been proposed on an isotropic growth process. The solvothermal reaction time, EG/H_2O volume ratio all play significant roles in the morphologies and sizes of the as-synthesized products. These phosphor particles exhibit a potential application in the display fields because of their special size, morphology and luminescence properties.

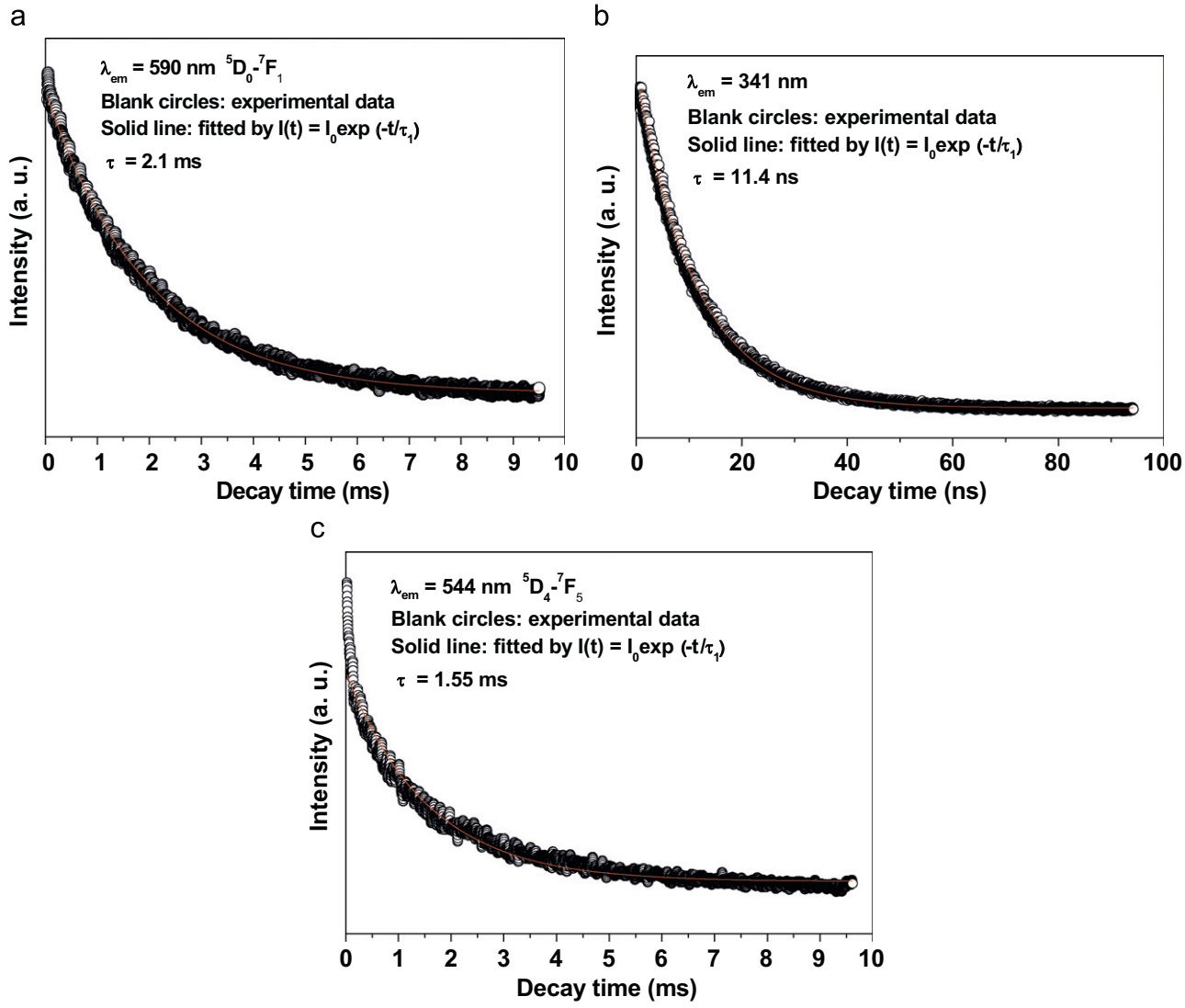

Fig. 10. The decay curves for $LaPO_4:Eu^{3+}$ (a), $LaPO_4:Ce^{3+}$ (b), and $LaPO_4:Ce^{3+}$, Tb^{3+} (c).

Acknowledgments

This project is financially supported by National Basic Research Program of China (2007CB935502) and the National Natural Science Foundation of China (NSFC 20871035, 50702057, 50872131, 00610227).

References

[1] C.T. Kresge, M.E. Leonowicz, W.J. Roth, J.C. Vartuli, J.S. Beck, Nature 359 (1992) 710.
[2] I.L. Radtchenko, G.B. Sukhorukov, N. Gaponik, A. Kornowski, A.L. Rogach, H. Mohwald, Adv. Mater. 13 (2001) 1684.
[3] D. Zhao, J. Feng, Q. Huo, N. Melosh, G.H. Fredrickson, B.F. Chmelka, G.D. Stucky, Science 279 (1998) 548.
[4] H. Yang, N. Coombs, G.A. Ozin, Nature 386 (1997) 692.
[5] P.V. Braun, P. Osenar, S.I. Stupp, Nature 380 (1996) 325.
[6] C.W. Guo, Y. Cao, S.H. Xie, W.L. Dai, K.N. Fan, Chem. Commun. (2003) 700.
[7] J. Liu, Y. Shin, Z. Nie, J.H. Chang, L.Q. Wang, G.E. Fryxell, W.D. Samuels, G.J. Exarhos, J. Phys. Chem. A 104 (2000) 8328.
[8] M.S. Fleming, T.K. Mandal, D.R. Walt, Chem. Mater. 13 (2001) 2210.
[9] R.A. Caruso, M. Antonietti, Chem. Mater. 13 (2001) 3272.
[10] F. Caruso, M. Spasova, V. Salgueirno-Maceria, Adv. Mater. 13 (2001) 1090.
[11] J. Yang, Z.W. Quan, D.Y. Kong, X.M. Liu, J. Lin, J. Cryst. Growth Des. 7 (2007) 730.
[12] Z.H. Jiang, C.Y. Liu, J. Phys. Chem. B 107 (2003) 12411.
[13] H. Sertchook, D. Avnir, Chem. Mater. 15 (2003) 1690.
[14] T. Ung, L.M. Liz-Marzan, P. Mulvaney, Langmuir 14 (1998) 3740.
[15] M. Giersig, T. Ung, L.M. Liz-Marzan, P. Mulvaney, Adv. Mater. 9 (1997) 570.
[16] X. Jing, T.G. Ireland, C. Gibbons, D.J. Barber, J. Silver, A. Vecht, G. Fern, P. Trogwa, D. Morton, J. Electrochem. Soc. 146 (1999) 4546.
[17] Y.C. Kang, I.W. Lenggoro, S.B. Park, K. Okuyama, Mater. Res. Bull. 35 (2000) 789.
[18] S.H. Cho, S.H. Kwon, J.S. Yoo, C.W. Oh, J.D. Lee, K.J. Hong, S.J. Kwon, J. Electrochem. Soc. 147 (2000) 3143.
[19] H. Wang, C.K. Lin, X.M. Liu, J. Lin, Appl. Phys. Lett. 87 (2005) 181907.
[20] B. Alken, W.P. Hsu, E. Matijevic, J. Am. Ceram. Soc. 71 (1988) 845.
[21] L. Xu, G. Guo, D. Uy, A. O'Neil, W.H. Weber, M.J. Rokosz, R.W. McCabe, J. Appl. Catal. B 50 (2004) 113.
[22] R.X. Yan, X.M. Sun, X. Wang, Q. Peng, Y.D. Li, Chem. Eur. J. 11 (2005) 2183.
[23] K. Rajesh, P. Mukundan, P.K. Pillai, V.R. Nair, K.G.K. Warrier, Chem. Mater. 16 (2004) 2700.
[24] C.C. Tang, Y. Bando, D. Golberg, R. Ma, Angew. Chem. Int. Edn. 44 (2005) 576.
[25] H.C. Lu, G.S. Yi, S.Y. Zhao, D.P. Chen, L.H. Guo, J.J. Cheng, Mater. Chem. 14 (2004) 1336.
[26] G.Y. Adachi, N. Imanaka, Chem. Rev. 98 (1998) 1479.
[27] F.H. Firsching, S.N. Brune, J. Chem. Eng. Data 36 (1991) 93.
[28] A. Rouanel, J.J. Serra, K. Allaf, V.P. Orlovskii, Inorg. Mater. 17 (1981) 76.
[29] Y. Guo, P. Woznicki, A. Barkatt, E.E. Saad, I.G. Talmy, J. Mater. Res. 11 (1996) 639.
[30] J. Dexpert-Ghys, R. Mauricot, M.D. Faucher, J. Lumin. 69 (1996) 203.
[31] G. Blasse, B.C. Grabmaier, Luminescent Materials, Springer, Berlin, 1994.
[32] R.P. Rao, D.J. Devine, J. Lumin. 87–89 (2000) 1260.
[33] N. Hashimoto, Y. Takada, K. Sato, S. Ibuki, J. Lumin. 48/49 (1991) 893.
[34] J. Dexpert-Ghys, R. Mauricot, M.D. Faucher, J. Lumin. 69 (1996) 203.
[35] X. Wu, H. You, H. Gui, X. Zeng, G. Hong, C. Kim, C. Pyun, B. Yu, C. Park, Mater. Res. Bull. 37 (2002) 2531.
[36] Y.W. Zhang, Z.G. Yan, L.P. You, R. Si, C.H. Yan, Eur. J. Inorg. Chem. (2003) 4099.

[37] Y.P. Fang, A.W. Xu, R.Q. Song, H.X. Zhang, L.P. You, J.C. Yu, H.Q. Liu, J. Am. Chem. Soc. 125 (2003) 16025.
[38] L.X. Yu, H.W. Song, S.Z. Lu, Z.X. Liu, L.M. Yang, X.G. Kong, J. Phys. Chem. B 108 (2004) 16697.
[39] H. Meyssamy, K. Riwotzki, A. Kornowski, S. Naused, M. Haase, Adv. Mater. 11 (1999) 840.
[40] C.R. Patra, G. Alexandra, S. Patra, D.S. Jacob, A. Gedanken, A. Landau, Y. Gofer, New J. Chem. 29 (2005) 733.
[41] B.Y. Ahn, S.I. Seok, S.I. Hong, J.S. Oh, H.K. Jung, W.J. Chung, Opt. Mater. 28 (2006) 374.
[42] M.J. Fisher, W.Z. Wang, P.K. Dorhout, E.R. Fisher, J. Phys. Chem. C 112 (2008) 1901.
[43] L. Zhu, X.M. Liu, X.D. Liu, Q. Li, J.Y. Li, S.Y. Zhang, J. Meng, X.Q. Cao, Nanotechnology 17 (2006) 4217.
[44] Z.L. Wang, Z.W. Quan, J. Jin, J.Y. Fang, J. Nanosci. Nanotechno. 5 (2005) 1532.
[45] H. Meyssamy, K. Riwotzki, A. Kornowski, S. Naused, M. Haase, Adv. Mater. 11 (1999) 840.
[46] J.C. Yu, L.Z. Zhang, Z. Zheng, J.C. Zhao, Chem. Mater. 15 (2003) 2280.
[47] J. Anderssona, S. Arevaa, B. Spliethoffb, M. Lindéna, Biomaterials 26 (2005) 6827.
[48] X. Peng, L. Manna, W. Yang, J. Wickham, E. Scher, A. Kadavanich, A.P. Alivisatos, Nature 404 (2000) 59.
[49] J.L. Zhang, G.Y. Hong, J. Solid State Chem. 177 (2004) 1292.
[50] J. Yang, Z.W. Quan, K.Y. Kong, X.Y. Liu, J. Lin, Cryst. Growth Des. 7 (2007) 730.
[51] C.X. Li, Z.W. Quan, J. Yang, P.P. Yang, J. Lin, Inorg. Chem. 46 (2007) 6329.
[52] M. Yu, J. Lin, J. Ju, J.J. Zhang, Y.C. Han, J. Mater. Chem. 13 (2003) 1413.
[53] Z.L. Wang, Z.W. Quan, J. Lin, J.Y. Fang, J. Nanosci. Nanotech. 5 (2005) 1532.